A. Pineau and P. Joly**

Local versus Global Approaches to Elastic–Plastic Fracture Mechanics. Application to Ferritic Steels and a Cast Duplex Stainless Steel

REFERENCE Pineau, A. and Joly, P., **Local versus global approaches to elastic–plastic fracture mechanics. Application to ferritic steels and a cast duplex stainless steel**, *Defect Assessment in Components – Fundamentals and Applications*, ESIS/EGF9 (Edited by J. G. Blauel and K.-H. Schwalbe) 1991, Mechanical Engineering Publications, London, pp. 381–414.

ABSTRACT The mechanical integrity of structures is usually characterised by means of several relatively well established rules based on a global approach of fracture, such as K or J. It is essentially assumed that fracture can be described in terms of a single parameter, K_{1C} or J_{1C}. This approach may yet be questionable in complex situations. This is one of the reasons why local approaches of fracture have also been developed. An attempt is made to review the application of these local approaches, especially those which are micromechanistically based. The paper is divided into two main parts.

The first part deals with low alloy ferritic steels. For cleavage fracture a statistical model based on the Weibull weakest link fracture theory is presented. For ductile rupture the emphasis is laid upon cavity growth nucleated from inclusions. In these materials it can be assumed that cavity nucleation takes place at a critical strain. The mechanics of plastic porous materials, in which the work hardening of the undamaged material is balanced by the softening effect due to void growth, is introduced. It is shown that ductile rupture can be modelled in terms of a critical void growth criterion. The statistical aspects of ductile rupture are also briefly discussed. These fracture criteria are then used to model fracture toughness. In particular it is shown that under large-scale yielding conditions the size requirement which must be fulfilled to determine a valid fracture toughness, J_{1C} depends not only on the specimen geometry but also on fracture micromechanisms.

The second part is an attempt to model ductile rupture of a cast duplex (ferrite and austenite) stainless steel. In this material, cavities are formed from cleavage cracks which are continuously initiated in the embrittled ferrite phase. An equation describing the variation of void growth and void nucleation is derived partly from quantitative metallography measurements. It is shown that the failure process of this material can also be modelled in terms of a critical porosity. The problems raised by the application of this fracture criterion established in a volume element to the crack tip situation are briefly discussed.

Introduction

The mechanical soundness of structures is usually ensured on the basis of several relatively well accepted rules. These rules are supposed to be able to assess the mechanical integrity for often complex engineering applications and complex loading conditions, including large-scale yielding, mixed cracking opening modes, and non-isothermal loading conditions. Rules based on elastic and elastic–plastic fracture mechanics have prevailed for the last 25 years, although such approaches may be questionable in numerous cases. The main

* Centre des Matériaux-Ecole des Mines de Paris, BP 87-91003 Evry Cedex, France.

problem which is raised is the transferability of laboratory test results to components. The standardisation of fracture toughness testing is presently undergoing rapid development. The standards for linear fracture toughness, K_{1c}, for example, are commonly accepted in spite of the fact that even under plain strain small-scale yielding there remains a size effect associated with the probability of finding a weak point along the crack front through the specimen thickness. The size requirements, in particular the ligament size, which must be fulfilled in an elastic–plastic fracture mechanics test in order to measure a 'valid' value of J_{1c} are still more problematic. In all these efforts in the standardisation of fracture mechanics tests, which are extremely useful, it is assumed that fracture toughness can be measured by a single global parameter, such as K or J.

More recently another approach to the problem has been developed. This is the local approach which relies upon the fact that it is possible to model macroscopic fracture behaviour in terms of local fracture criteria. These criteria are established from a modelisation of the fracture micromechanisms in a specific material which are investigated in a volume element before being applied to the crack tip situation. Therefore the development of this methodology requires that at least two conditions are fulfilled.

(1) Micromechanistically based models for a given physical process of fracture must be developed.
(2) A perfect knowledge of the stress–strain field in front of stationary and propagating cracks is required. This has been made possible by the advent of analytical and numerical solutions. To this effect the global and local approaches of fracture are more complementary than contradictory. It is clear that the recent progress in the numerical analysis methods, in particular the finite element method (FEM), has largely contributed to the development of the local approach.

This paper is divided into two main parts. The first is devoted to a brief description of local criteria for ductile and brittle fracture and to the application of these criteria for the prediction of fracture toughness. This part is mainly based upon the work of the Beremin research group. A fuller account of the results has already been published **(1)–(5)**. These results were obtained on a low alloy C–Mn–Ni–Mo steel (A508) used in the fabrication of pressurised water reactors. The second part of the paper is devoted to a duplex stainless steel which is also used in the piping equipment of nuclear reactors. This part is more prospective since the study is not yet completed. However an attempt is made to show how various tools which are developed in the local approach of fracture can be applied to this complex material.

Brief description of local criteria for brittle and ductile fracture of ferritic steels

These criteria were established from tests and observations carried out on notched round tensile bars. Several geometries were used in order to investi-

gate the effect of stress triaxiality on both cleavage fracture and ductile rupture. These specimens were calculated by finite element method. In most of these calculations it was assumed that damage has no effect on the constitutive equations of the material.

Cleavage fracture

The micromechanisms of cleavage fracture have been reviewed by several authors (see, for example, **(1)**). In a steel for which there is no change in deformation modes with temperature, that is, cleavage is always slip induced, it can be assumed that brittle fracture takes place when the maximum principal stress reaches a critical value, σ_c. Several models have been proposed to account for the value of σ_c ($\simeq$1500 MPa in structural steels). One important aspect of brittle fracture is the existence of a relatively large scatter in the results. This situation, very well known in ceramic materials, does not seem to have been given enough attention in steels for a long time. For a homogeneous material in which there is no statistical spatial correlation between two adjacent areas, the Weibull weakest link concept **(6)** is well accepted to account for brittle fracture. This was the basis of the model proposed by Beremin **(3)** and Wallin *et al.* **(7)**. In this theory the probability of failure, P_R, of a specimen of volume V subjected to an homogeneous stress state, σ is given by

$$P_R = 1 - \exp\left(-\frac{\sigma^m V}{\sigma_u^m V_u}\right) \tag{1}$$

Where V_u is an arbitrary unit volume, σ_u is the average cleavage strength of that unit volume while m is the Weibull exponent. Equation (1) is a simplified expression since no cut-off parameter is introduced. In three dimensions and in the presence of smooth stress gradients, this equation can be expressed as:

$$P_R = 1 - \exp\left(\frac{\int_{pz} \sigma_1^m \, dv}{\sigma_u^m V_u}\right) \tag{2}$$

where σ_1 is the maximum principal stress and the volume integral is extended over the plastic zone PZ. The latter expression can be rewritten as

$$\sigma_w = \sqrt[m]{\left(\int_{pz} \sigma_1^m \frac{dv}{V_u}\right)} = \sigma_u \sqrt[m]{\left(\ln \frac{1}{1 - P_R}\right)} \tag{3}$$

where σ_w is referred to as the 'Weibull stress'.

The procedures used to determine the parameters σ_u, m, and V_u are given in detail elsewhere **(2)–(5)**. The values of σ_u and m are determined from tests carried out on notched bars. In a bainitic C–Mn–Ni–Mo steel (A508) it was found that $m = 22$, while σ_u was dependent on the microstructure of the material **(3)**. A similar value of m was measured in a welded C–Mn steel **(8)**. The results obtained on the latter material are reproduced in Fig. 1, where a good agreement is observed between the experiments and equation (3). Recent

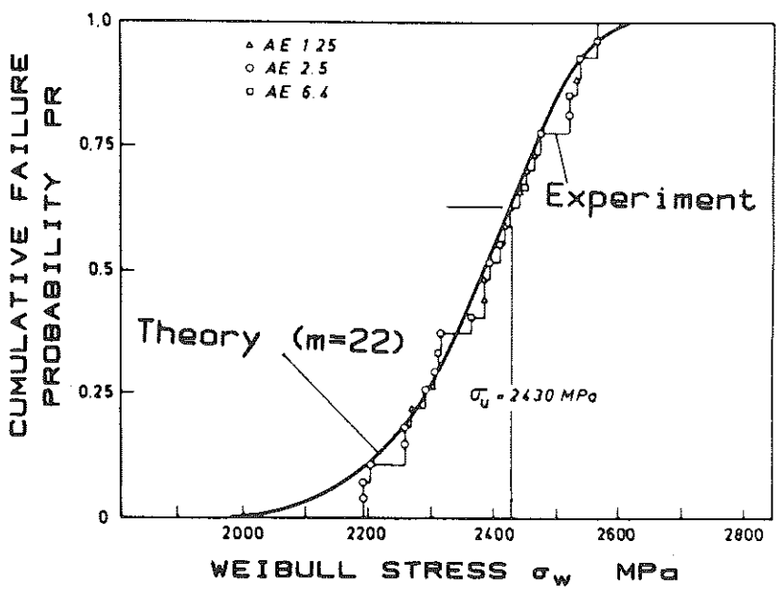

Fig 1 Welded C–Mn steel. Probability of cleavage fracture as a function of Weibull stress. Comparison between experiment and calculations (equation (2)) (8)

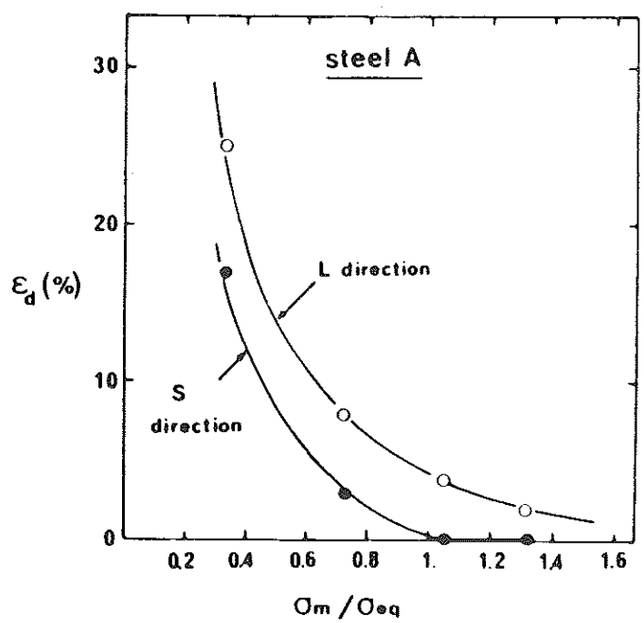

Fig 2 A 508 steel. Heat A (%S = 100 ppm). Tensile tests on notched specimens. Critical strain to nucleate cavities from MnS inclusions as a function of stress triaxiality ratio σ_m/σ_{eq}. Effect of orientation. (11)

results obtained on a pearlitic rail steel indicate that larger values of m can be obtained **(9)**. The volume V_u is determined from valid K_{1c} tests carried out at low temperature. This volume V_u is introduced as the characteristic distance (a few grain sizes) used in the Ritchie, Knott, and Rice model **(10)**.

Ductile fracture

Critical porosity at failure

In most structural steels, ductile fracture arises from the nucleation, the subsequent growth, and coalescence of cavities initiated from inclusions. In the next section devoted to a cast stainless steel it is shown that the nucleation sites may be different. The stress state has an influence on the three steps of ductile fracture. This was investigated in some detail on various heats of a C-Mn-Ni-Mo steel containing different volume fractions of inclusions by using axi-symmetrically notched specimens. The details are given elsewhere **(2)(11)(12)**.

In this material the mechanisms of cavity nucleation are dependent on the orientation. In the longitudinal direction cavities are formed by the fracture of MnS inclusions, while in the transverse directions cavities are nucleated from the de-cohesion of the interface between MnS particles and the matrix. The aspect ratio of the inclusions related to the amount of hot deformation applied to the material was also shown to be important. The results obtained on one heat which contained 100 ppm of sulphur are shown in Fig. 2, where it is observed that at large stress triaxiality ratio ($\sigma_m/\sigma_{eq} \gtrsim 1$) cavity nucleation takes place at very small strain ($\lesssim 5$ percent). It was shown that cavity formation from MnS inclusions in A508 steel obeys a critical stress criterion similar to the expression proposed by Argon *et al.* **(13)** which can be expressed as

$$\sum_1 + k(\sigma_{eq} - \sigma_0) = \sigma_d \tag{4}$$

where $\sum_1$ is the maximum principal stress, σ_{eq} is the von Mises equivalent stress, σ_0 is the yield strength, while k and σ_d are temperature independent parameters which are functions of the inclusion shape.

Several models have been proposed to model cavity growth. For an infinite body and at large stress triaxiality factors the expression derived by Rice and Tracey **(14)** can be written as

$$dR/R = \alpha\, d\varepsilon_{eq} \exp(1.5\sigma_m/\sigma_{eq}) \tag{5}$$

where R is the actual size of the cavities which have an initial size R_0, $d\varepsilon_{eq}$ is the increment of equivalent plastic strain, σ_m is the mean stress, while α is a proportionality factor which is close to 0.28. Very few experiments have been carried out to test the validity of this theory. In a model material in which Al_2O_3 inclusions were purposely introduced it was shown that equation (5) describes very well the experimental results, except for the proportionality factor α which was shown to be much larger than 0.28 **(12)**. The comparison

between different materials showed that α was an increasing function of the volume fraction of inclusions. Therefore the interactions between inclusions might explain this effect. Another explanation might also relate in the fact that in steels, especially around large inclusions, a second population of cavities initiated from carbides takes place. This effect has been investigated recently by Perrin and Leblond **(15)** using the Gurson model for porous material which is described in the following.

Equation (5) can be used to assess the critical void growth at failure R_c/R_0 which is obtained by integrating this expression along the stress–strain path in the centre of notched specimens calculated by finite element method. A number of results obtained on four heats of A508 steel are given in Fig. 3. These results indicate that at fracture the values of R_c/R_0 are very small even in the longitudinal direction. Typically the initial volume fraction occupied by the inclusions is increased by a factor much lower than one order of magnitude. For a given material and a given orientation it is observed that R_c/R_0 is a slightly decreasing function of stress triaxiality ratio. A simple model was proposed in which a larger stress triaxiality dependence was predicted **(1)**. This difference is thought to be related to the fact that when testing sharply notched specimens to introduce large stress triaxiality ratios the volume of material submitted to critical conditions is smaller compared to specimens tested at lower stress triaxiality. This size effect which is related to the statistical aspects of ductile fracture should deserve more detailed studies. In the following section devoted to a cast material, this important aspect is emphasised.

In summary, in a material in which cavity nucleation takes place easily and at large stress triaxiality ratio, the ductile fracture of a volume element can be described in terms of a critical void growth ratio, R_c/R_0. The fact that R_c/R_0 is, within a first approximation, a constant largely simplifies the analysis since,

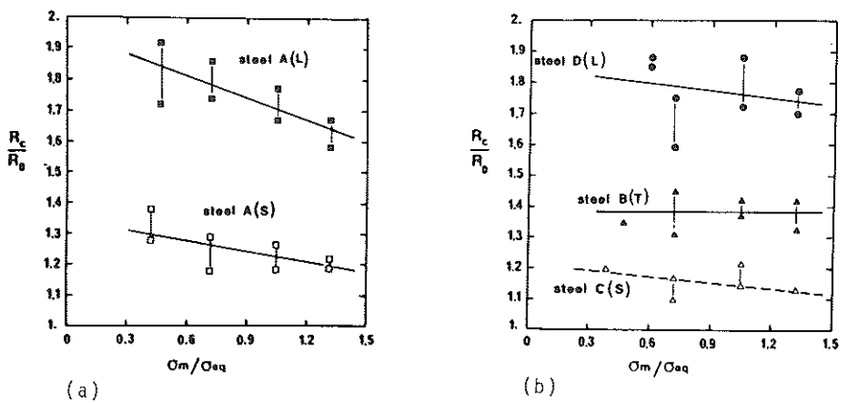

Fig 3 A 508 steel. Heat A (%S = 100 ppm); Heat B (%S = 200 ppm); Heat C (%S = 130 ppm); Heat D (%S = 50 ppm). Effect of stress triaxiality ratio on critical void growth, R_c/R_0. Influence of orientation. (11)

as shown in Fig. 4, the ductility at failure, ε_c is largely dependent on stress triaxiality ratio.

Mechanics of plastic porous materials

A large research effort has been developed over the last past decade to model the strain softening effect produced by growing cavities in a matrix which is plastically deformed. In these models the plastic flow potential is dependent on cavity volume fraction. In principle this coupling effect introduced between damage and the constitutive equations can be used to model flow localisation and rupture. A full description of the existing theories is out of the scope of this paper. Here we refer only to the Gurson and the Rousselier models.

The yield criterion introduced by Gurson **(16)** is written as

$$\sigma_{eq}^2/Y^2 + 2f\cosh(3\sigma_m/2Y) - 1 - f^2 = 0 \tag{6}$$

where Y is the flow stress of the matrix. The dependence of the yield criterion upon the mean stress, σ_m gives rise, through the associated flow rule, to a hydrostatic component in the plastic strain from which the increase in the volume fraction of cavities is deduced. Tvergaard **(17)** suggested introducing some additional parameters q_1, q_2, q_3 by which equation (6) can be re-written as

$$\sigma_{eq}^2/Y^2 + 2q_1 f\cosh(3q_2\sigma_m/2Y) - 1 - q_3 f^2 = 0 \tag{7}$$

which $q_1 \simeq 1.5$, $q_2 \simeq 1$, and $q_3 \simeq q_1^2$. For small volume fractions, the Gurson expression can be written as

$$\sqrt{(3/2s_{ij}s_{ij})} = Y[1 - 0.50f\exp(3\sigma_m/2Y)] \tag{8}$$

In this expression the softening effect due to the presence of porosities is clearly noticed, especially for large stress triaxialities. The associated increment

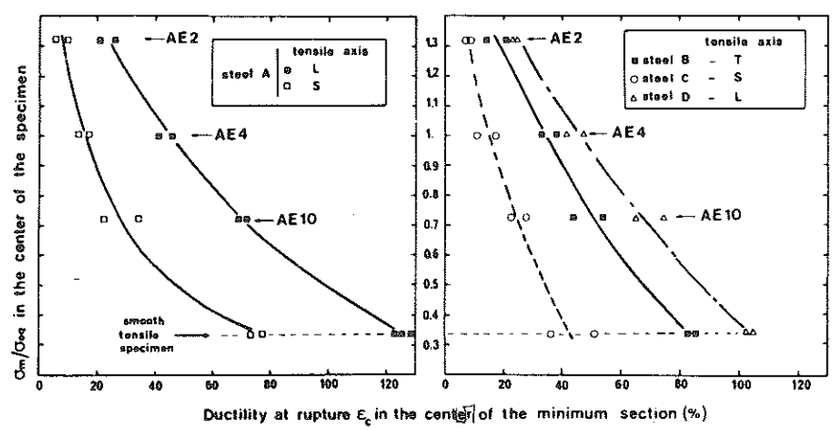

Fig 4 A 508 steel. Ductility at fracture as a function of stress triaxiality ratio. Influence of orientation. AEX refers to a notched specimen with a notch radius of X (in mm) (see Fig. 14(a)). (11)

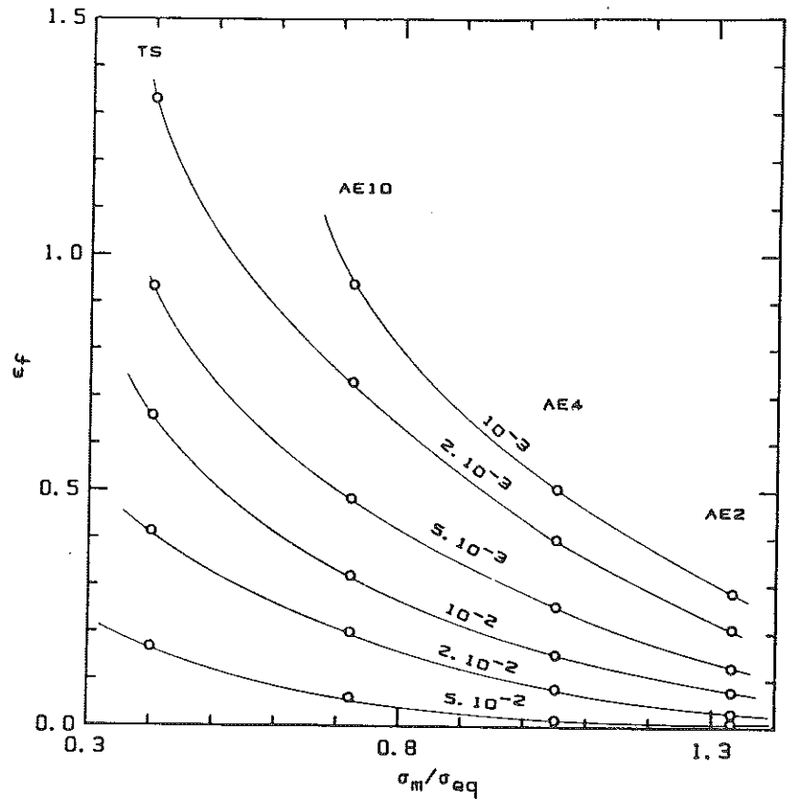

Fig 5 Theoretical variation of ductility with stress triaxiality ratio (20). **The numbers indicated on the curves refer to various values of f_0/n ratio**

in cavity volume fraction is given by

$$d\varepsilon_{ii} = df/(1-f) = 0.75f.\ \exp(3\sigma_m/2Y)\ d\varepsilon_{eq} \tag{9}$$

which is very similar to the Rice and Tracey expression (equation (5)), except for the proportionality factor which is equal to 3×0.28 instead of 0.75.

The application of the Gurson–Tvergaard potential has been reviewed recently by Needleman **(18)**. In the simulation of ductile fracture it was observed that this model largely overestimated the ductility measured in structural materials. The function f^* was proposed by Tvergaard and Needleman **(19)** to account for the effects of rapid void coalescence at failure. Initially $f^* = f$, as originally proposed by Gurson but, at some critical void fraction, f_c the dependence of f^* on f is increased in order to simulate a more rapid decrease in strength as the voids coalesce. This model therefore bears a strong resemblance to the critical void growth criterion introduced in the previous section.

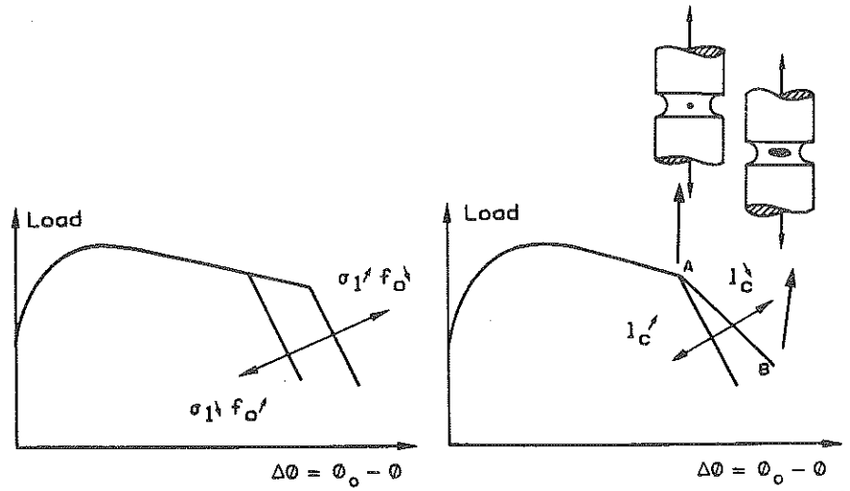

Fig 6 Sketch showing the softening effect associated with damage (a). Influence of σ_1 and f_0 (equation (11)); (b) Influence of mesh size, l_c

Mudry **(20)** has also attempted to use the Gurson potential without the accelerating effect in f introduced by Tvergaard and Needleman **(19)** to simulate the ductility of various heats of A508 steel. For a homogeneous distribution of inclusions this author showed also that the calculated ductilities were much larger than those which were measured. Moreover a too large stress triaxiality dependence on ductility was observed. This suggested that the statistical effects were also important as indicated previously. To investigate this effect Mudry **(20)** assumed that the inclusions were distributed according to a Poisson law. The results of his calculations are given in Fig. 5 where it is observed that, within a first approximation, the variation of the ductility, ε_c with stress triaxiality ratio is only dependent on the ratio between the initial volume fraction of inclusions, f_0 and the work-hardening exponent, n of the stress–strain curve written as

$$\sigma = K\varepsilon^n \tag{10}$$

In Fig. 5 only the curves corresponding to a probability to failure of 50 percent are drawn. However it was noticed that the difference between the curves corresponding to $P_R = 0.10$ and $P_R = 0.90$ was small. Roughly speaking the local volume fraction in the cell which gives rise to the failure of the specimen can be as large as 5 or 10 times the mean volume fraction, as already underlined by other authors **(1)(21)(22)**.

The yield function introduced by Rousselier **(23)(24)** was established from the thermodynamics of continuous media. It can be written as

$$\sigma_{eq}/(1-f)Y = 1 - DB(\beta)/Y.\ \exp[\sigma_m/(1-f)\sigma_1]$$

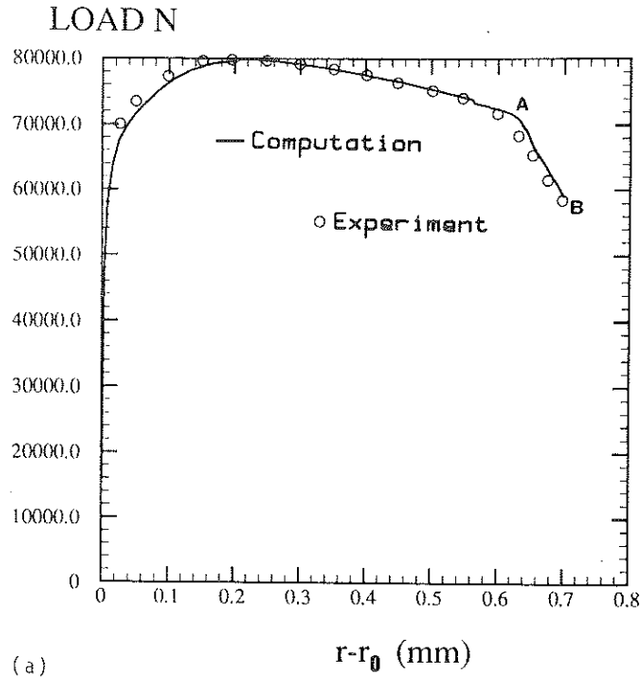

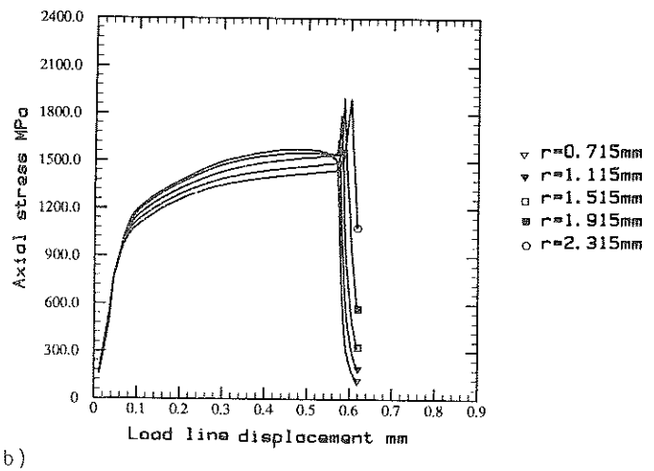

Fig 7 Cr–Ni–Mo steel. Results of finite element method calculations of notched ($\rho = 5$ mm) specimens. (a) Comparison between the calculated and the measured (24) load-displacement curve. (b) Variation of axial stress at various locations in the minimum section of the specimen with load line displacement

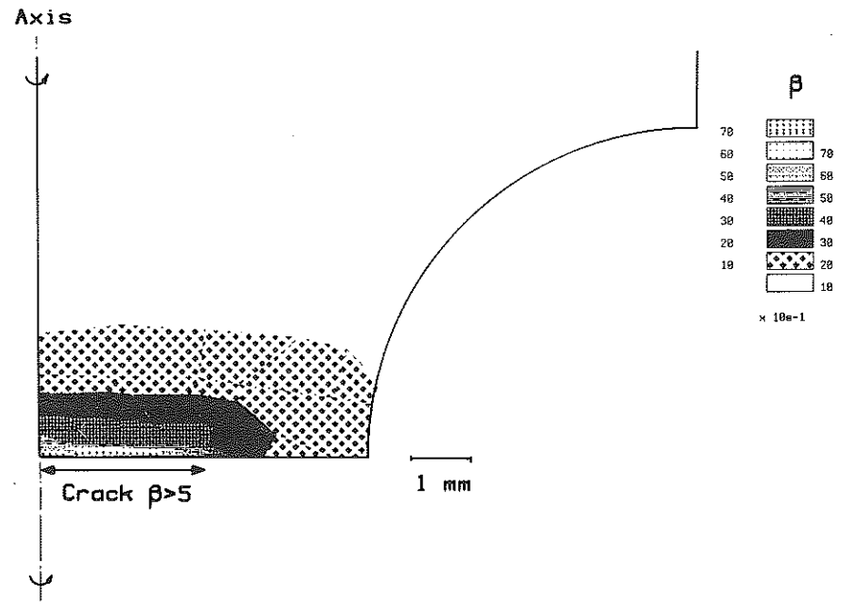

Fig 8 Cr-Ni-Mo steel. Calculated damage as represented by β parameter (equation (11)) across the notch section determined at failure (B in Fig. 7(a))

with

$$d\beta = df/f(1-f) = D \exp\left[\sigma_m/(1-f)\sigma_1\right] d\varepsilon_{eq} \tag{11}$$

and

$$B(\beta) = \sigma_1 fo \exp \beta/(1 - f_0 + f_0 \exp \beta)$$

This criterion also bears a strong analogy with the Gurson model and with the Rice and Tracey expression provided it is assumed that $D = 3 \times 0.28$ and $\sigma_1 = 2/3Y$. Rousselier introduced his criterion in a finite element code to simulate the failure of notched bars as indicated in Fig. 6. In this figure the effect of σ_1 and f_0 parameters as well as the influence of the mesh size of the elements, l_c located in the centre of the specimens are indicated. In particular it was shown that this method of coupling between damage and constitutive equations was extremely efficient to simulate not only crack initiation taking place at A, which is dependent on σ_1 and f_0, but also crack growth corresponding to the slope of the branch AB of the loading curve which is dependent on the l_c parameter. The Rousselier criterion was introduced recently in the Ecole des Mines Zébulon finite element code. The validity of this implementation was tested by simulating the failure of a Cr-Mo steel notched bar which was studied previously by Rousselier (**24**). This simulation was done with the following parameters $D = 2$, $\sigma_1 = 490$ MPa and

$l_c = 0.4$ mm. The diameter of the minimum section of the section is $\phi_0 = 10$ mm, while the notch radius is 5 mm. The stress–strain curve is defined by $Y = 974\ \varepsilon^{0.06}$. The initial volume fraction of cavities, f_0 is equal to $2\ 10^{-4}$. Figure 7(a) shows that the simulated and the experimental loading curve are very close to each other. The softening effect associated with cavity growth is observed in Fig. 7(b), while the distribution of damage represented by the values of β is shown in Fig. 8. It is worth noting that in this simulation which contains no accelerating factor in cavity growth, in contrast to the previous model, large values of β, i.e. large values of initial cavity growth are found.

Application to the prediction of fracture toughness

Characteristic distances and local criteria

At the crack tip, as in many models based on local criteria, it is necessary to introduce a characteristic distance, λ over which strains and stresses are averaged. In FEM calculation this size is used for the first element located at the crack tip. The mesh size is related to the material properties, in particular its microstructure and not necessarily to the conditions for a precise numerical solution. Theoretically the introduction of a coupling effect between damage and constitutive equations could help in the solution of this difficult problem.

For brittle fracture it was indicated previously that the distance λ, or the unit volume V_u in the Weibull statistics is determined from valid fracture toughness tests carried out at low temperature. For ductile rupture the characteristic distance is related to the mean inclusion spacing, for instance the mean spacing in a plane perpendicular to the crack front when ductile tearing is modelled as a two-dimensional process. It can therefore be assumed that

$$\lambda \simeq 1/2\sqrt{(N_a)} \tag{12}$$

where N_a is the number of inclusions per unit area in this plane. It was shown that this definition of λ provided satisfactory results and that at crack initiation the crack tip opening displacement, CTOD was of the order of λ **(11)**.

In order to take the effect of inclusion distribution into account, a mean value for the cavity growth ahead of a crack tip can be calculated as

$$\langle R/R_0 \rangle = \int_0^\infty R/R_0(x/\mathrm{CTOD}, \theta) \cdot P(x, \theta) \cdot \mathrm{d}V(x) \tag{13}$$

where $P(x, \theta)$ is the probability of finding one inclusion in the volume $\mathrm{d}V$ defined in Fig. 9. The void growth rate, R/R_0, at a given position (x/CTOD, θ) can be calculated using the results of FEM calculations in which crack blunting effect was taken into account **(25)(26)**. The choice of the length, h, along the crack front is critical. For materials in which the inclusions are homogeneously distributed, h was defined as

$$h = (N_{AL} N_{AT} N_{AS})^{1/3}/N_v \tag{14}$$

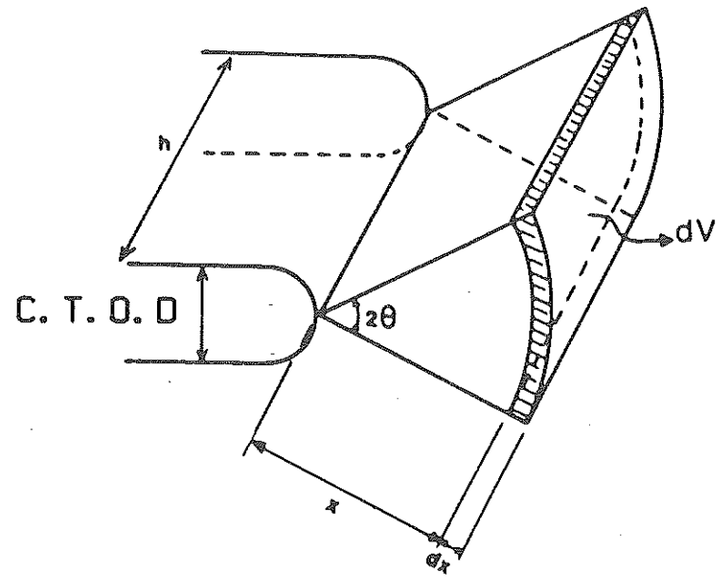

Fig 9 Definition of the elementary volume in front of a crack tip

where N_{AL}, N_{AT}, and N_{AS} represent the number of inclusions per unit area in a plane perpendicular to the longitudinal, transverse, or short transverse direction, respectively, while N_v is the number of inclusions per unit volume. The mean value of the calculated void growth $\langle R/R_0 \rangle$ was compared to the critical cavity growth rate R_c/R_0 determined from tests carrried out on notched bars (see e.g. Fig. 3). From this the theoretical CTOD at crack initiation was determined. The comparison between the calculated and the experimental values is shown in Fig. 10 where the results obtained on four steels tested in various directions are given. A good agreement is observed except for material C which contained a large volume fraction of inclusions (%S = 130 ppm) and which was tested in the short-transverse direction. SEM observations showed that the inclusions were grouped into colonies. The influence of void clusters is examined more thoroughly in the next section devoted to a cast duplex stainless steel.

Theoretical expressions between J_{1c} or K_{1c} and local criteria under small-scale yielding conditions

Using known analytical solutions for the crack tip stress–strain field (HRR field **(27)(28)**) in conjunction with FEM plane strain small-scale yielding results to model the crack tip blunting effect it is possible to derive theoretical relationships between the fracture toughness, K_{1c} or J_{1c} and the local criteria.

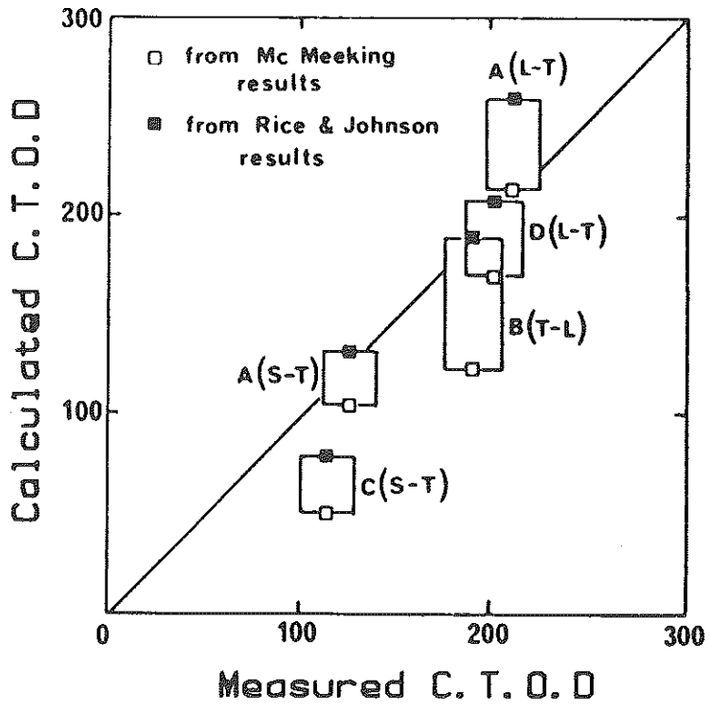

Fig 10 A 508 steel. Heats A, B, C, D. S content indicated in Fig. 2. Comparison between calculated (equation (13)) and measured values of crack tip opening displacement (CTOD) (11)

For brittle fracture, the expression of the 'Weibull' stress was derived previously **(3)**. From this the probability for cleavage fracture can be expressed as

$$P_R = 1 - \exp\left(-\frac{J_{1c}^2 E^2 B \sigma_0^{m-4} C_m}{(1-\nu^2) V_u \sigma_u^m}\right) \tag{15}$$

where B is the specimen thickness, E the Young modulus and C_m is a numerical factor. As shown earlier **(3)(29)(30)**, the predicted variations of K_{1c} with specimen size and temperature – via the temperature dependence of the yield strength – are in good agreement with the experiment results.

For ductile rupture, similarly it was shown that J_{1c} at crack initiation is related to critical void growth $(R/R_0)_c$ by the following expression

$$J_{1c} = \alpha\lambda\sigma_0 \ln (R/R_0)_c \tag{16}$$

where α is also a numerical factor.

Fracture toughness under large-scale yielding conditions

The effect of specimen geometry and specimen size on ductile tearing resistance J_R curves is now well documented. A number of experimental results

show that J_R curves are dependent on specimen thickness, in-plane dimensions and, in particular on the mode of loading, tension versus bending (see e.g. **(31)–(33)**). The lower J_R curves are obtained with CT specimens and the steeper curves with CCP specimens. Side grooving of test pieces which tends to reduce the surface shear lip effect does not eliminate totally the influence of specimen geometry, which controls the plastic constraint effect in the plane of the specimen. In order to overcome this difficulty there is an effort in the test standardisation to dictate a size requirement such that the specimen ligament size, b is larger than $N(J/\sigma_0)$ with $N \simeq 25$ for CT specimens and $\simeq 200$ for CCP specimens. These requirements are independent on the failure micromechanisms. This is a research area where the local approach of fracture can be extremely useful to test the validity of such rules.

A recent study was devoted to this problem **(34)**. Both CT and CCP specimens were calculated under plane strain conditions using finite element method. A power law expression (equation (10)) was used to describe the stress–strain behaviour of the material. Two widely different values for the work-hardening exponent were used, $n = 0.005$ and $n = 0.10$. Moreover the influence of crack length was tested as indicated in Table 1. In this study two local failure criteria, one for cleavage fracture (equation (3)), and the other one for ductile rupture, R_c/R_0 were used to simulate numerically crack initiation. The results corresponding to ductile rupture are shown in Fig. 11 where the product $\lambda \ln (R/R_0)_c$ introduced in equation (16) is plotted as a function of J/σ_0. As indicated previously under small-scale yielding conditions, there is no effect of specimen size or specimen geometry. On the other hand it is noticed that the relation between $\lambda \ln (R/R_0)$ and J/σ_0 is largely specimen dependent when general yielding is reached. The results show that the values of J_{1c} are larger in CCP specimen than in CT specimens. Moreover the values of J_{1c} are dependent on the work-hardening exponent.

These results were extended to predict the influence of in-plane dimensions. It is well to remember that in this analysis the three-dimensional effects related to thickness effects, which may also play an important role, are not taken into account. The details are given elsewhere **(34)**. The results related to size

Table 1 Specimen geometries and materials characteristics

Specimen No	*Geometry*	*a/W*	*Strain hardening Exponent*
53	CT	0.45	0.10
54	CT	0.60	0.10
55	CT	0.45	0.005
56	CT	0.60	0.005
258	CCP	0.75	0.10
259	CCP	0.45	0.10
268	CCP	0.75	0.005
269	CCP	0.45	0.005

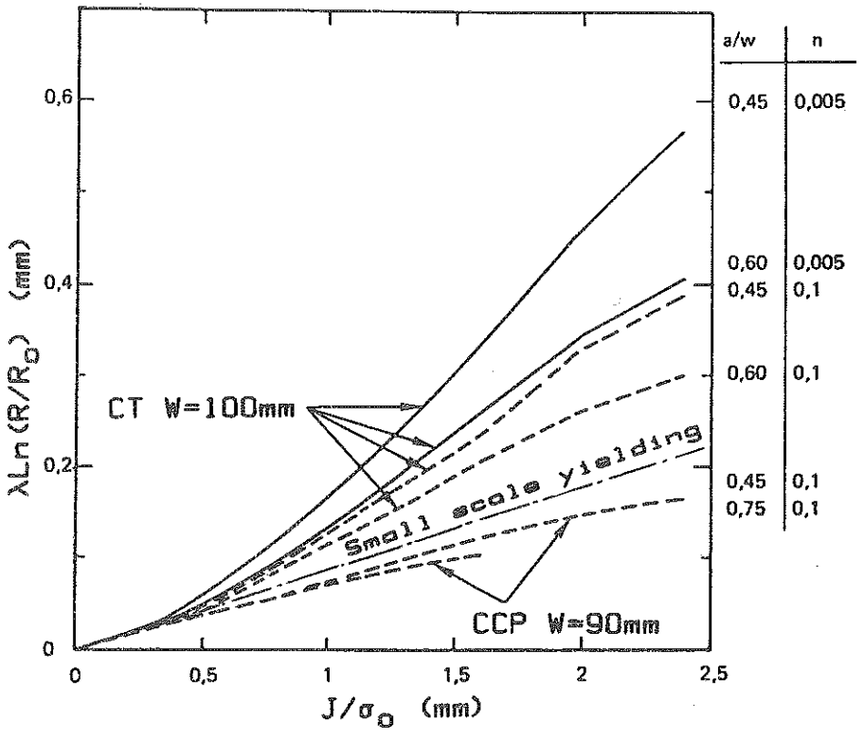

Fig 11 Variation of the ductile rupture criterion as a function of the loading parameter J/σ_0. Influence of specimen geometry and work hardening exponent (34)

requirements are reported in Table 2. The values of the N factor introduced previously were obtained by using a deviation of 10 percent from the small-scale yielding solution. Table 2 shows that it is difficult to define a universal value for the minimum size requirement since it is dependent on the micro-mechanisms of failure. For cleavage fracture the values of N derived from this

Table 2 Minimum size requirement for J_{1c} measurements

	Minimum $b\sigma_0/J$ for valid J_{1c}	
Specimen N_0	*Cleavage Fracture*	*Ductile Rupture*
53-CT	20	140
54-CT	15	85
55-CT	28	155
56-CT	40	90
258-CCP	185	25
259-CCP	990	30
268-CCP	560	45
269-CCP	1650	50

analysis are close to those recommended for fracture toughness tests. Larger values for CCP specimens reflect the fact that cleavage fracture is essentially stress controlled. Conversely for ductile rupture which is essentially a strain-controlled process the size requirements are less stringent for CCP specimens than for CT specimens.

More recently Rousselier *et al.* (35) have also used a local approach to simulate both crack initiation and stable crack growth in various specimen geometries, including not only CT and CCP types but also Single Edge Cracked Panel (SECP) specimens. The Rousselier model which is based on damage mechanics was presented previously. This model for ductile rupture was applied to one heat of a cast duplex stainless steel which is investigated more thoroughly in the next section. The results of these numerical simulations are given in Fig. 12, where a large effect of specimen geometry is observed in spite of the fact that, in these conditions, the large-scale yielding conditions were not reached.

These studies show therefore that the minimum size requirements which have to be fulfilled to measure a valid fracture toughness, J_{1C} are extremely

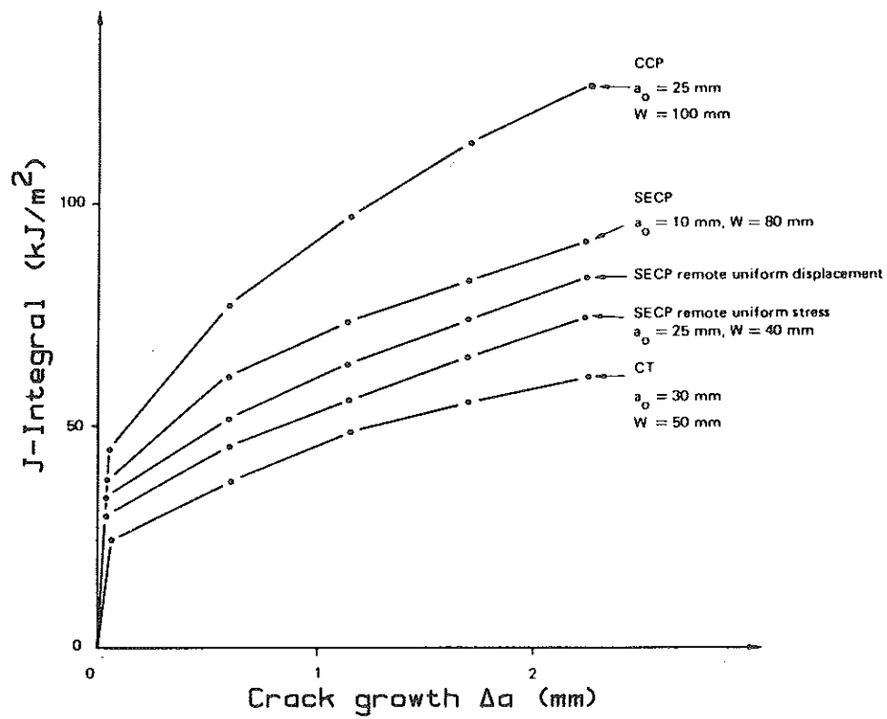

Fig 12 Calculated crack growth resistance curves. Influence of specimen geometry and size (35)

difficult to establish unless the mechanisms of fracture are properly described, both experimentally and numerically.

Damage and fracture toughness of an embrittled cast duplex stainless steel

Introduction

It is well established that duplex austenitic-ferritic stainless steels (CF8 and CF8M) containing from 10 percent to 25 percent ferrite are embrittled at the service temperature (320°C) of pressurised water reactors, see e.g. **(36)–(38)**. The ferrite phase submitted to the well-known '475°C embrittlement' is strengthened by the formation of α' and other precipitates **(39)**. A number of studies have been made to characterise the kinetics of the embrittlement effect by using the results of Charpy impact and tensile tests carried out on materials which were aged for various times at different temperatures. From this an apparent activation energy was determined and used to define an equivalence between temperature and time of embrittlement **(36)(37)**.

Reactor integrity analysis requires the determination of fracture toughness properties. The transferability of fracture toughness values obtained on small laboratory test specimens raises the problem of geometrical and size effects, as discussed previously. In these cast materials which have a very coarse microstructure the question is still more problematic as compared to ferritic steels. The aim of this study, therefore, is to investigate the micromechanisms of damage and fracture of an aged cast duplex stainless steel and to provide the basis of a local approach for predicting fracture toughness.

Material

The material under investigation was taken from a centrifugally cast CF8M stainless steel pipe (Heat Y4331). It contains approximately 20 percent ferrite. The chemical composition is given in Table 3. The material was first annealed at 1115°C and then aged at 400°C for 700 hours. This resulted in a decrease of the Charpy impact energy KC_v measured at room temperature from about 200 J/cm^2 down to 30 J/cm^2. After ageing the yield strength and the UTS measured in the tangential direction of the pipe was 323 MPa and 717 MPa, respectively.

Figure 13 shows the microstructure of this material observed on three perpendicular planes. A complex structure consisting of a ferrite network (dark grey) surrounded by austenite (white) is noticed. The ferritic network is formed by fine platelets (thickness $\simeq$ 20 μm) connected on long distances ($\simeq$1 mm). At

Table 3 Chemical composition (Wt percent) of the cast CF8M stainless steel investigated

C	*N*	*Mn*	*Si*	*Ni*	*Cr*	*Mo*	*Cu*	*Co*	*Nb*	*S*	*P*
0.04	0.044	0.76	1.17	10.03	20.80	2.56	0.15	0.05	0.19	0.001	0.023

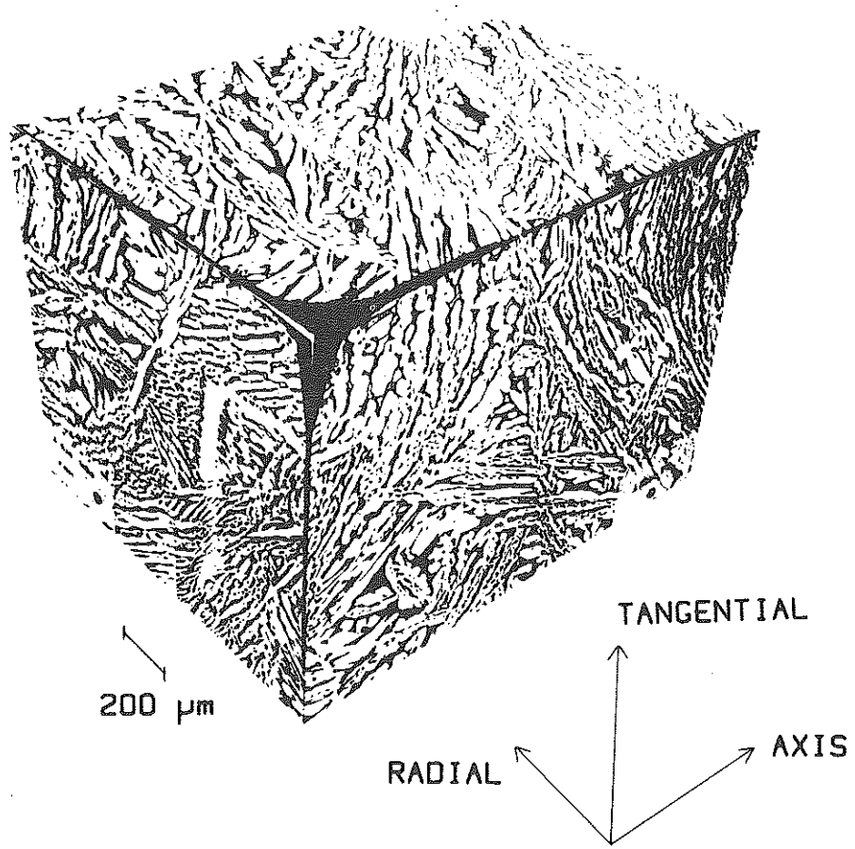

Fig 13 Cast duplex CF8M stainless steel. Optical micrograph of three perpendicular planes

a larger scale macrographic etching showed a structure of large 'grain' units ($\sim$1 mm width and from several mm to 1 cm length) elongated in the radial direction and surrounded by a relatively wide ($\sim$50 μm) ribbon of austenite. Microhardness measurements (50 g) showed a large difference between both phases: 187 HV in the austenite phase compared to 616 $\pm$ 120 HV in the ferrite phase.

Damage micromechanisms of volume element

Experimental procedures

Tensile tests were carried out at room temperature and a strain rate of 3.10^{-3} s^{-1} on smooth and notched bars (Fig. 14(a)), oriented as indicated in Fig. 14(b). The smooth specimens were instrumented with a longitudinal extensometer of 25 mm gauge length. The notched bars were tested with a diametral

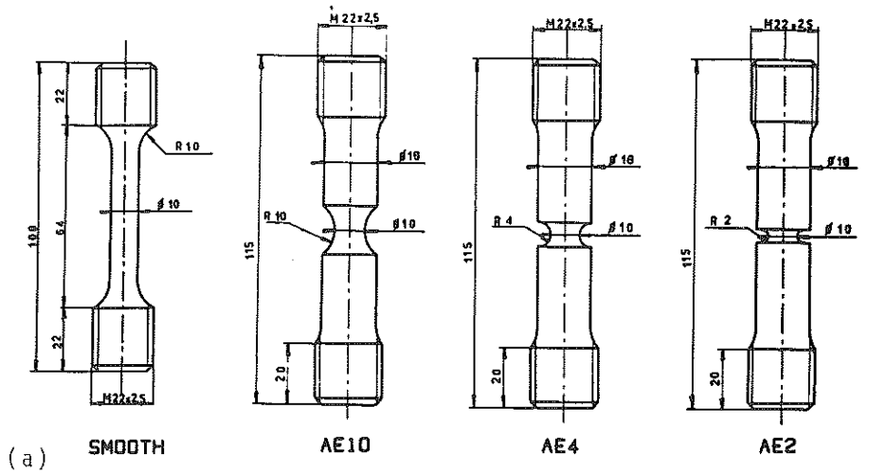

(a)

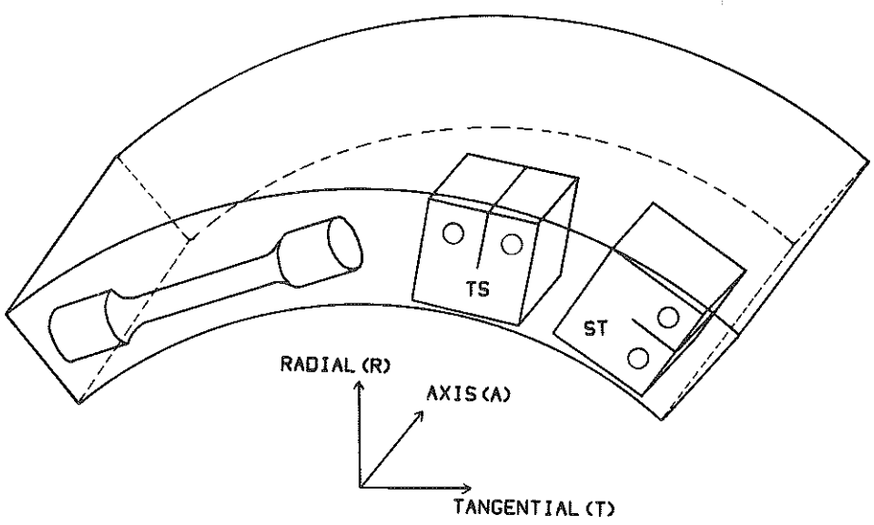

(b)

Fig 14 (a) Specimen geometry. All dimensions in mm; (b) Specimen orientation

extensometer measuring the minimum diameter of the notch in the radial direction of the pipe, from which the mean strain was defined as $\bar{\varepsilon} = 2 \log (\phi_0/\phi)$ where $\phi_0 = 10$ mm is the initial diameter and ϕ the actual value.

The specimens were calculated by FEM using the SYSTUS code developed by Framatome. A von Mises yield criterion was used. The true stress–strain

curve determined from a tensile test was introduced point by point. The details of these calculations are given elsewhere **(40)**.

A large number of metallographical and fractographic observations were made to investigate the deformation patterns of both austenite and ferrite. In particular, to determine the position and the number of cleavage cracks in the ferrite phase, longitudinal sections of both smooth and notched bars were made on a plane perpendicular to the radial direction of the pipe. These sections were examined at a magnification of $\times 60$. To determine the size distribution of these cleavage cracks the samples were carefully polished and then slightly etched. These observations were made at a magnification of $\times 400$. The microcrack lengths were measured on both planes perpendicular to the radius and to the axis of the pipe.

Results and discussion

The variation of the ductility measured by $\bar{\varepsilon}$ at failure, $\bar{\varepsilon}_f$ as a function of stress triaxiality ratio, σ_m/σ_{eq} at the centre of the specimen, determined from FEM calculations is shown in Fig. 15. It is worth noting that the ductility is low compared to an unembrittled material for which $\bar{\varepsilon}_f \simeq 1.10$ for $\sigma_m/\sigma_{eq} \simeq 0.60$. The dependence of $\bar{\varepsilon}_f$ with σ_m/σ_{eq} is moderate as observed for the ductile rupture of sulphur-rich ferritic steels tested in the short transverse direction (steel C, Fig. 4(b)).

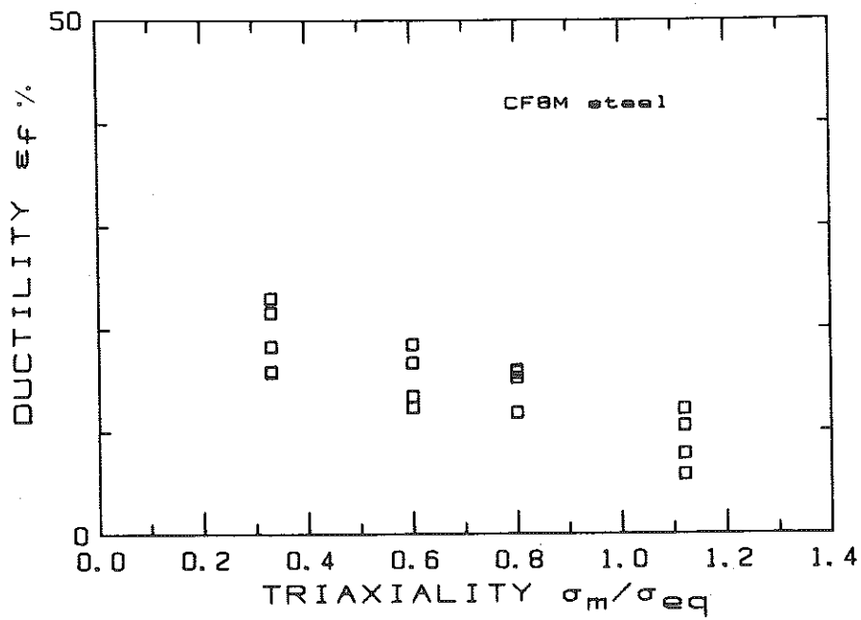

Fig 15 CF8M steel. Ductility of smooth and notched specimens as a function of stress triaxiality ratio

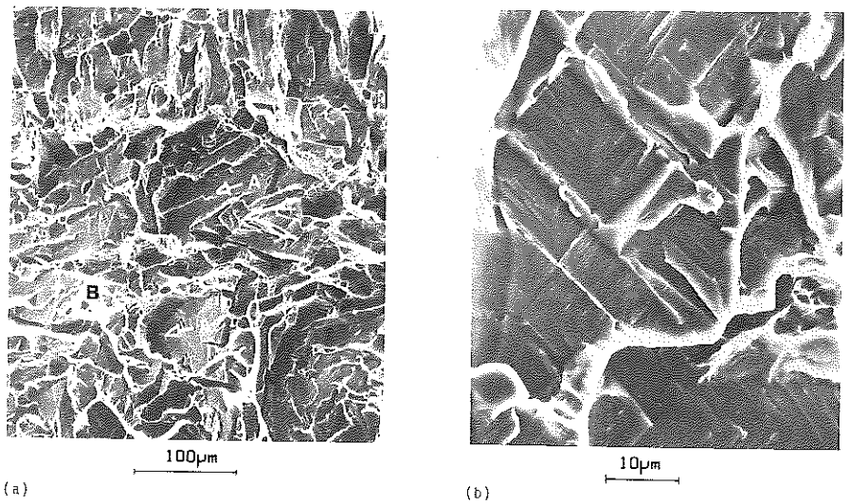

Fig 16 CF8M steel. SEM fractograph. (a) General aspect of the fracture surface showing cleaved ferrite areas (A) and ductile austenite walls (B); (b) detail of cleaved area in the ferrite phase

Fractographic observations show large areas of transgranular cleavage in ferrite forming large 'dimples' linked together by vertical austenite 'walls' containing very fine and elongated dimples likely formed on small carbides (Fig. 16(a)). At larger magnification typical crystallographic patterns are observed (Fig. 16(b)). They were interpreted as resulting from mechanical twinning.

Longitudinal sections showed that both austenite and ferrite phases were plastically deformed (Fig. 17.) Thick deformation bands which were identified as mechanical twins by TEM **(41)** are observed in particular at the phase boundary between austenite and ferrite (Fig. 17(a)). Deformation bands are also observed in ferrite. SEM observations on a polished free surface showed that deformation in this phase occurred by pencil glide. However, coarser deformation bands were also observed in the ferrite phase (Fig. 17(b)). An analysis of the angles between these lines suggested that they could be related to mechanical twinning taking place also in ferrite. This suggestion was confirmed by TEM observations **(41)**.

Cleavage cracks are nucleated in ferrite as shown in Fig. 17. In most cases they completely cross the ferrite islands, although a number of them were observed to be arrested within the ferrite. These microcracks are then blunted by plastic deformation of austenite forming a triangular vertex (Fig. 18). This figure suggests that in this material the nucleation stage of cavities formed by cleavage microcracks is a continuous process. A detailed analysis of the location of the nucleation sites in notched specimens showed no drastic influence of the macroscopic principal stress on the onset of cleavage crack nucleation.

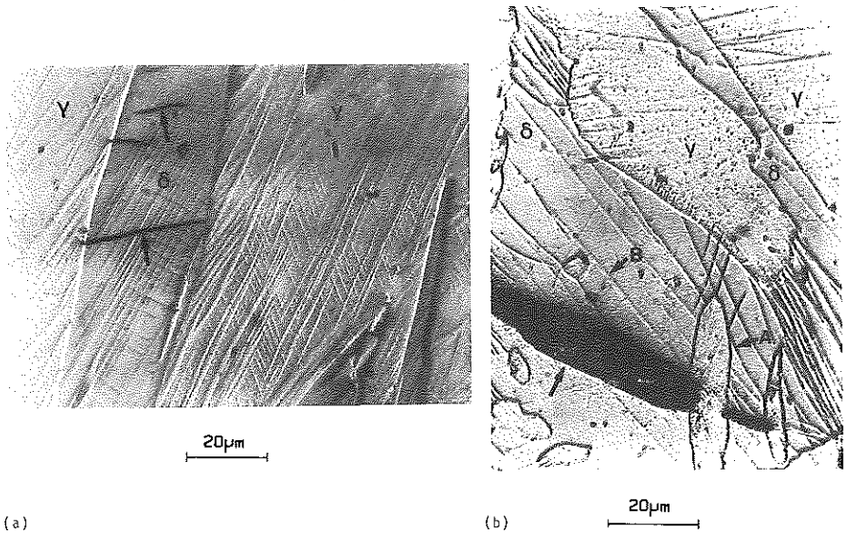

Fig 17 CF8M steel. Optical micrographs of a strained ($\varepsilon = 18.3$ percent) tensile specimen. Deformation patterns in austenite (γ) and ferrite (δ) phases. (a) Deformation bands in austenite and cleavage cracks (arrows) in ferrite; (b) Sinuous (A) and planar (B) deformation bands in ferrite. Large cavity grown from a cleavage crack in the ferrite phase (arrow)

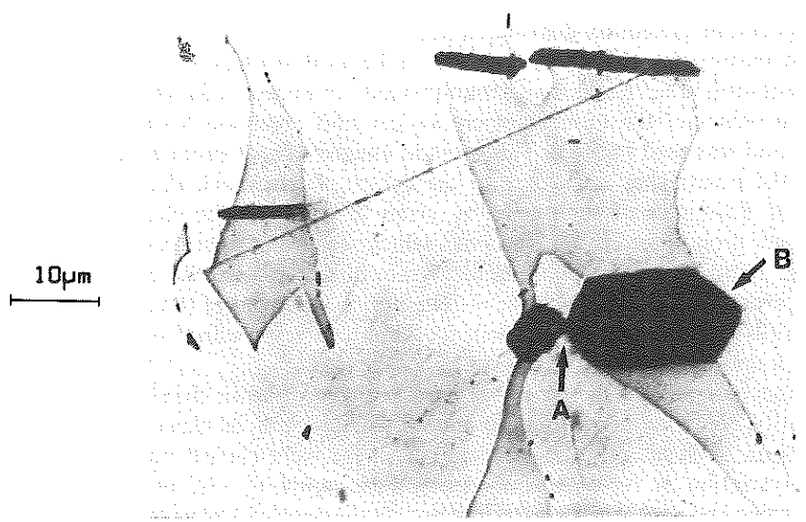

Fig 18 CF8M steel. Optical micrograph. Cavity growth and coalescence in A. Note vertex-shaped crack blunting in B

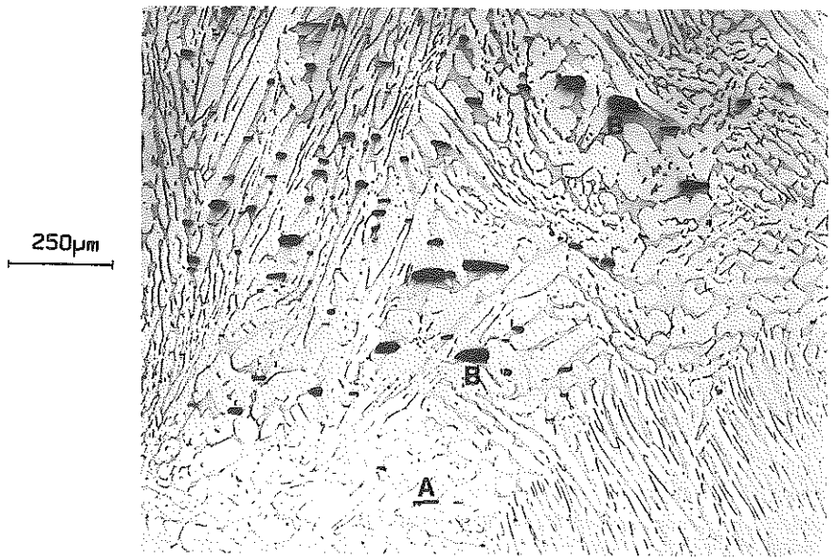

Fig 19 CF8M steel. Optical micrograph showing a cluster of cavities initiated in ferrite phase. Note the difference in enlargement of cavities (A and B, for instance)

It was observed that the first cleavage cracks were formed at a low applied strain ($\sim$2 percent).

As stated previously another difficulty encountered in this cast material is associated with the fact that cavities initiated from ferrite cleavage cracks are very inhomogeneously distributed and form clusters in specific grains (Fig. 19). The reasons for this clustering effect (chemical segregation, crystallographic orientation of ferrite, and austenite phases) are under study. In order to define local values of the number of cracks per unit area, the Voronoï tesselation method was used **(42)(43)**. This method assigns to each crack a cell containing all the points that are closer to the centre of this crack than to any other crack. Examples of such cells are given in Fig. 20. The clustering effect is largely pronounced in the specimen which was given a strain of $\sim$16 percent (Fig. 20(b)). The corresponding histogram of the cell size shows that although the average crack density is $\bar{N}_a = 16.6\ \text{mm}^{-2}$, 4 percent of the area is occupied by cells with an area lower than 0.01 mm^2 corresponding to local values of crack density larger than 100 mm^{-2}.

The comparison of Fig. 20(a) and Fig. 20(b) shows that the local crack density, N_a, is an increasing function of plastic strain, as expected. Interrupted tests on both smooth and notched specimens were carried out to investigate the variation of N_a with equivalent plastic strain ε^P_{eq}. N_a was measured by counting the number of cracks in a square element of 1 mm^2 while in notched specimens, the local values of ε^P_{eq} were determined from FEM calculations. The results are shown in Fig. 21. This figure shows that the nucleation rate should

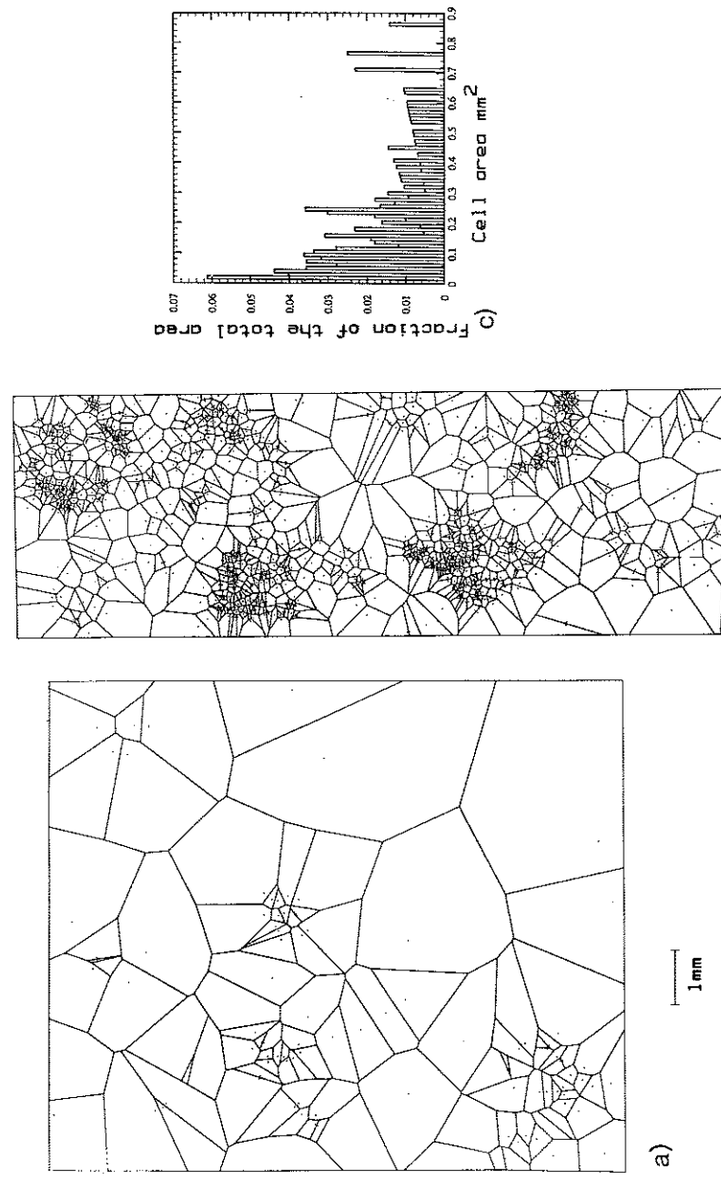

Fig 20 CF8M steel. Damage measurements in smooth bar (a) $\varepsilon = 8.9$ percent; (b) $\varepsilon = 15.8$ percent. Voronoï cells. (c) Distribution of cell size after $\varepsilon = 15.8$ percent

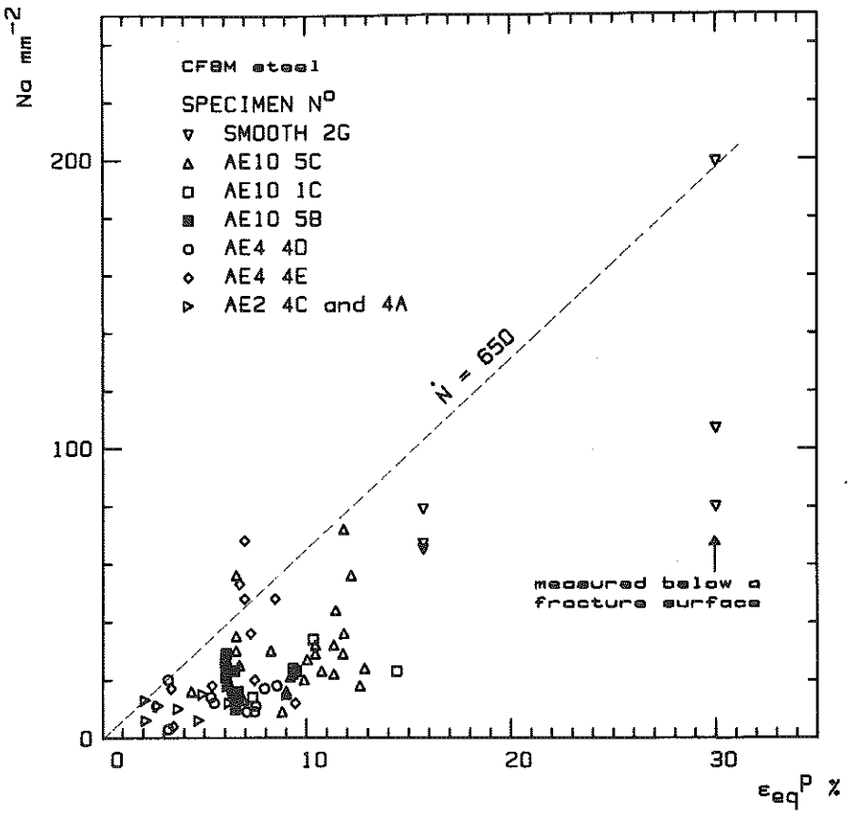

Fig 21 CF8M steel. Crack density as a function of strain. Measurements on smooth and notched specimens

be given a statistical meaning. A study is under progress to investigate this specific aspect. In this paper we define a maximum nucleation rate corresponding to $\dot{N}_a = 650\ \text{mm}^{-2}$. This value means that for $\varepsilon_{eq}^P = 0.16$, $N_a = 104$ and only 4 percent of the total area can exhibit higher nucleation rate (Fig. 20(c)).

As in ductile rupture of ferritic seels these measurements can now be used to assess the volume fraction of cavities at failure. The increment of porosity, df, has two origins, the growth of existing cavities and the nucleation of new ones, such that it can be written as

$$df = df_g + df_n \tag{17}$$

Assuming that df_g obeys the Rice and Tracey law and that the nucleation rate is constant and equal to A_n, equation (17) can be rewritten as

$$df/d\varepsilon_{eq} = 3 \times 0.28 \exp(3\sigma_m/2\sigma_{eq}) f(1-f) + A_n \tag{17}$$

For small f, neglecting second order terms, this expression leads, after integration, to

$$f = A_n/K(\exp K\varepsilon - 1) \tag{18}$$

with $K = 3 \times 0.28 \exp(3\sigma_m/2\sigma_{eq})$.

The determination of A_n involves both the measurement of $\dot{N}_a$ in a plane, for instance the plane perpendicular to the radial direction of the pipe and the measurement of cavity sizes in two perpendicular planes. Assuming that a flat cavity is as damaging as a sphere of the same projected area in a plane perpendicular to the tensile axis, see e.g. **(11)(20)** and that the cracks shape is elliptical, stereological calculations lead to

$$\dot{f}_N = \tfrac{1}{3}\dot{N}_{aR} \cdot \bar{Z}_A(\bar{D}_R \bar{D}_A)^{3/2} \tag{19}$$

where D_i is the actual size of a crack in a direction i, and $\bar{Z}_i = \overline{(1/d_i)}$, where d_i is the size of a crack measured in a section i. All the cracks are assumed to be perpendicular to the tensile axis. Thus the constant A_n in equation (18) is given by

$$A_n = 1/3\bar{Z}_A(\bar{D}_R \bar{D}_A)^{3/2}\, dN_a/d\varepsilon_{eq} \tag{20}$$

Taking $dN_A/d\varepsilon_{eq} = 650\ \text{mm}^{-2}$, $\bar{D}_R = 22.3\ \mu\text{m}$, and $\bar{D}_A = 7.3\ \mu\text{m}$, which were determined from metallographic observations, it is found that $A_n = 4.42\ 10^{-2}$.

An approach similar to that developed for ductile rupture of ferritic steels can now be used by integrating equation (17) to define the critical void volume fraction at failure, f_c. In Fig. 22(a) we have reported the values of f_c calculated according to equation (18), taking for ε_c the mean ductility at failure $\bar{\varepsilon}_f$ and for σ_m/σ_{eq} the value of the stress triaxiality ratio at the centre of the notched specimens. This figure shows that f_c seems to be a slightly decreasing function of stress triaxiality as already noticed for R_c/R_0 (see Fig. 3). It is also worth noting that the critical porosity at failure is rather small ($f_c \simeq 0.5$–1 percent) which is also in qualitative agreement with the observations relative to porous materials made in the previous section. Beyond the explanation given in the previous part, in particular the size effect which is believed to play a dominant role in this type of material, like in many cast materials with a coarse microstructure, several factors might explain the small variation of f_c with stress triaxiality. Firstly, numerical calculations indicate that a large part of f_c ($\sim$80–90 percent) is due to cavity nucleation instead of conventional cavity 'growth'. It is quite conceivable that in this material cleavage crack nucleation is promoted by increasing stress triaxiality and maximum principal stress. Secondly the variations of f_c along the radius of the notched specimens should also be considered. These variations are shown in Fig. 22(b). It is observed that the specimens AE10 and AE4 exhibit a rather homogeneously distributed damage, as expected, while the more sharply notched AE2 specimens are more damaged near the notch than in the centre. Actually longitudinal sections of

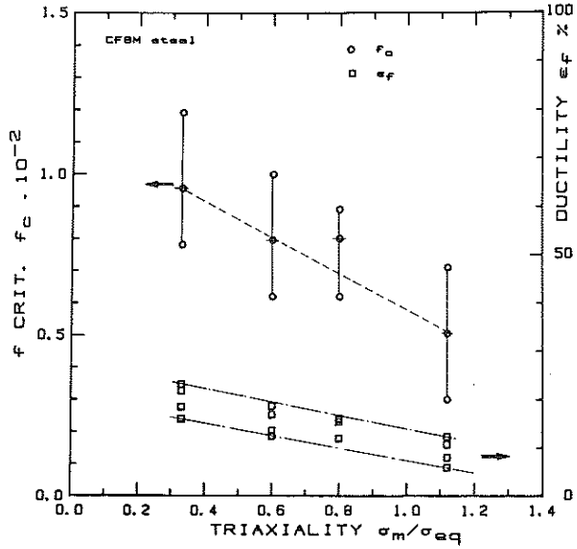

(a)

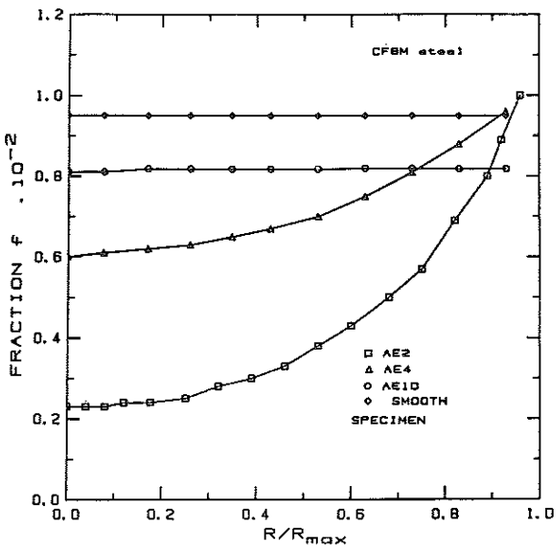

(b)

Fig 22 CF8M steel. (a) Variation of critical void fraction calculated from equation (18) and ductility as a function of stress triaxiality; (b) Distribution of calculated void fraction at failure along specimen radius

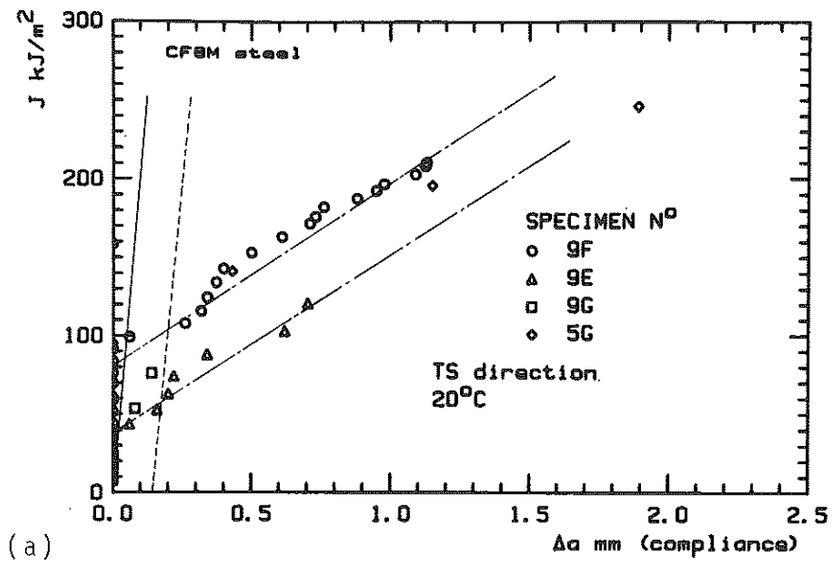

(a)

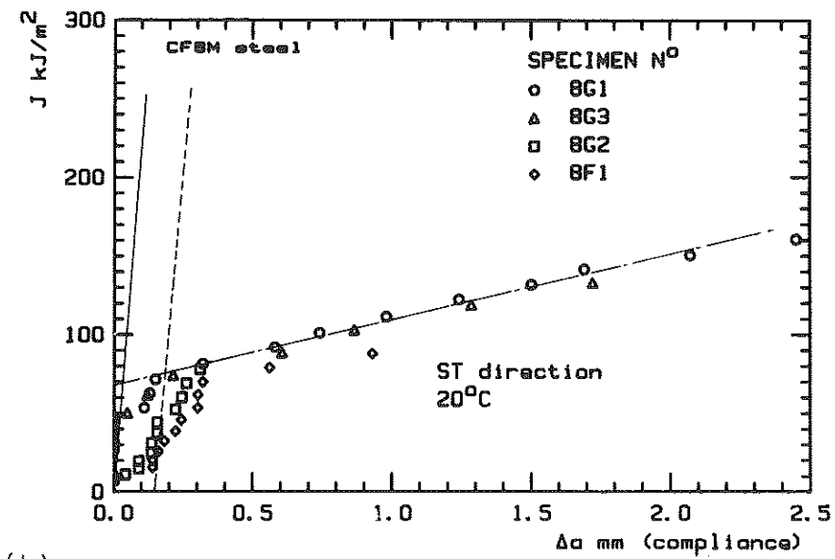

(b)

Fig 23 CF8M steel. Ductile crack growth resistance curves determined in (a) TS orientation; (b) ST orientation

interrupted tests showed that final failure could take place near the notch throat of AE4 and AE2 specimens.

To summarise, this analysis indicates that a critical value for the porosity at failure $f_c \simeq 0.8$ percent calculated from equation (18) might be a reasonable criterion to simulate the ductile rupture of cast CF8M stainless steel associated with the growth of cavities initiated from cleavage cracks induced in the ferrite phase by the inhomogeneity in deformation between both phases. It is also worth adding that this value of f_c is in qualitative agreement with the value inferred from the mechanics of porous materials. The work-hardening exponent n of our material is close to 0.28. This leads to $f_0/n \simeq 3.10^{-2}$. Figure 5 shows that for this value of f_0/n ratio low values of ductility similar to those which were measured are predicted. One of the main differences with the ductile rupture of more conventional materials is related to the continuous nucleation of damage sites which has to be taken into account.

Fracture toughness

Experimental procedure

J resistance curves were determined using CT type specimens with a thickness $B = 22.5$ mm, and in-plane dimension, $W = 30$ mm. They were fatigue precracked up to a ratio $a/W \simeq 0.6$. Then the specimens were side-grooved such that $B_N = 18$ mm. The EGF standards **(44)** were used to calculate J. The method of partial unloading was also used to determine the actual crack length. Optical crack extension was also determined after heat tinting according to the EGF method.

J_{IC} was determined by intersecting the blunting line, calculated as $J = 4\sigma_{flow}\Delta_a$ where $\sigma_{flow} = (R_{p0.2} + \text{UTS})/2$, shifted of $\Delta_a = 0.15$ mm, with the straight line drawn through the data points. Some tests were interrupted near initiation. Sections perpendicular to the crack front were performed to measure crack tip opening displacement at initiation (CTOD). Two orientations were investigated, ST and TS (see Fig. 14(b)).

Results and discussion

For both orientations, the J–Δa curves are given in Fig. 23(a) and (b). In the TS direction J_{IC} is between 50 and 100 kJ/m^2 and $dJ/da \simeq 110$ MPa, while, in the ST orientation, J_{IC} is close to 80 kJ/m^2 and $dJ/da \simeq 40$ MPa. There is not a strong anisotropy effect on toughness, but the ST direction seems to exhibit a lower tearing modulus. In both cases, initiation, detected by compliance method and with an electric potential drop method, took place close to the maximum of the P–δ curve, when the limit load was reached.

On one specimen of the TS orientation that had been interrupted at initiation, 6 sections were made in a plane perpendicular to the crack front (Fig. 24). A blunted fatigue crack front and cavities can be observed. The cavities are nucleated from cleavage cracks ahead of the crack tip. Propagation already took place over a distance of about 0.1 mm. In some cases, propagation occurred by initiating a new crack ahead of the main crack front. A metallographical procedure **(11)** was used to measure CTOD, when the blunted fatigue crack tip could clearly be defined. It was found that CTOD at crack initiation is equal to 43 ± 12 μm.

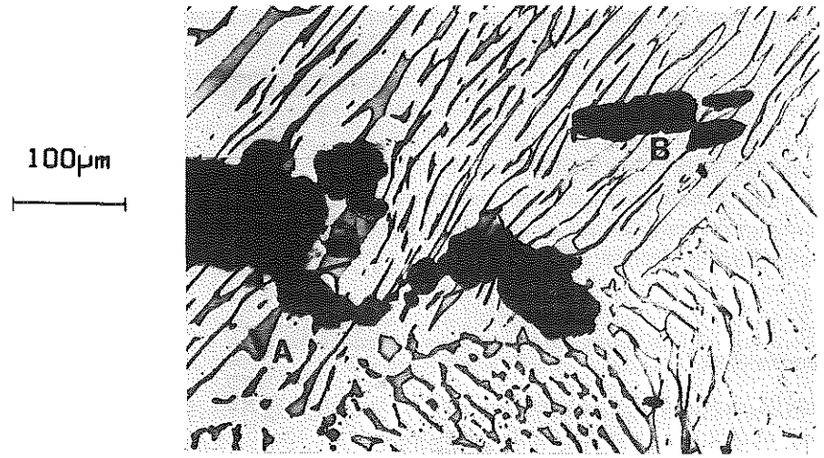

Fig 24 CF8M steel. Optical micrograph illustrating nucleation of cleavage cracks (A), cavity growth (B) and coalescence with blunted crack tip

It is well known that there is a relationship between J_{IC} and CTOD that can be written as

$$J_{IC} = M\sigma_y(\text{CTOD}) \tag{21}$$

Taking $J_{IC} = 80$ kJ/m^2, $\sigma_y = 320$ MPa and (CTOD) = 43 μm, equation (21) leads to $M = 5.8$. McMeeking **(26)** derived a theoretical expression where

$$M = \frac{1}{0.54(1+n)}\frac{2}{\sqrt{3}}\left\{(1+\nu)(1+n)\frac{\sigma_y}{nE}\right\}^{-n} \tag{22}$$

where n is the work hardening coefficient assuming that, at large plastic strains, the stress–strain relation is written as $\sigma = K(\varepsilon_p)^n$. Taking $n = 0.285$, $\nu = 0.3$, $E = 190\,000$ MPa, one finds $M = 6, 2$, which is a value in rather good agreement with the experimental value of 5.8.

The application of the local approach for predicting the fracture toughness of this material is still under investigation. It is believed that a sound analysis requires more metallographical and statistical information related in particular to the distribution of the clusters of damage shown previously. This information could be used to calculate the mean volume fraction of cavities ahead of

the crack tip following a procedure similar to that used previously (equation (13)). Here it can only be stated that by using the results of FEM calculations published by McMeeking **(26)** in conjunction with the damage law given by equation (18) it is found that the calculated void volume fraction, f reaches a value of approximately 0.3 10^{-2} at a distance of about 1.1 CTOD from the crack tip. This value is of the same order of magnitude although lower than the value obtained on volume elements. However, it is clear that this cannot be regarded as a criterion since no metallurgical distance or no averaging procedure are introduced.

Conclusions

Ductile rupture of a volume element is described as the successive stages of void nucleation, growth, and coalescence. For the first two stages, criteria established for MnS inclusions in ferritic steels are given. In these materials it can be assumed that there exists a critical strain, which is a function of stress triaxiality ratio, to initiate cavities. On the other hand, in other materials, such as cast duplex stainless steels, void nucleation must be modelled as a continuous process. Taking into account this phenomenon, when necessary, the ductile rupture of a given material takes place for a critical porosity which is assessed from tests carried out on notched specimens. The mechanics of porous materials is a very promising tool to model the softening effect associated with void nucleation and their subsequent growth.

Statistical aspects play a key role in both ductile rupture and cleavage fracture. In ferritic steels the later mode of failure is reasonably well described by the Weibull weakest link theory. The statistical analysis of ductile rupture is not so well documented. In particular the formation of damage clusters, shown in a cast duplex stainless steel, as well as their interactions, should deserve more attention.

Simple expressions relating either the crack tip opening displacement (CTOD) or the J-integral to local criteria established for either ductile rupture or cleavage fracture are given. These expressions apply when the small-scale yielding condition are prevailing. On the other hand, under large-scale yielding conditions, the approach based on local criteria suggests that the ligament size required for determining valid fracture toughness values, independent of the specimen in-plane dimensions and geometry, is very much dependent on the failure micromechanism and, therefore, on the form of the damage law used to model the fracture process. In both modes of failure, stress triaxiality plays an important role. In ductile rupture which is essentially strain-controlled, the influence of stress triaxiality results not only from void growth, but also from cavity nucleation, especially when this process takes place continuously as in cast duplex strainless steel. Cleavage fracture is essentially dependent on the distribution of maximum principal stress.

Acknowledgements

This study is partly supported by Framatome and the 'Service de Contrôle et de Sureté des Installations Nucléaires'. The authors would like to acknowledge also many fruitful discussions with Dr Y. Meyzaud from Framatome.

References

(1) PINEAU, A. (1981) Review of fracture micromechanisms and a local approach to predicting crack resistance in low strength steels, *Proceedings 5th Int. Conf. on Fracture*, Cannes (Edited by D. François), Pergamon Press, **2**, 533–577.
(2) BEREMIN, F. M. (1981) *Met. Trans.*, **12A**, 723.
(3) BEREMIN, F. M. (1983) *Met. Trans.*, **14A**, 2277–2287.
(4) MUDRY, F. (1983) Methodology and applications of local criteria for the prediction of ductile tearing, *Elastic–Plastic Fracture Mech.* (Edited by M. H. Larsson), *4th ISPRA Conf.*, ISPRA, Italy, 263.
(5) MUDRY, F. (1983) Cleavage fracture and transition: application to the warmprestress effect, *Ibid.*, 303.
(6) WEIBULL, W. (1951) *J. Appl. Mech.*, **18**, 293–297.
(7) WALLIN, K., SAARIO, T., and TORRONEN, K. (1984) *Metal Science*, **18**, 13–16.
(8) FONTAINE, A., MAAS, E., and TULOU, J. (1987) *Nucl Engng Des.*, **105**, 83–88.
(9) JEUNEHOMME, S. and FONTAINE, A. Private communication.
(10) RITCHIE, R. O., KNOTT, J. F., and RICE, J. R. (1973) *J. Mech. Phys. Solids*, **21**, 395.
(11) LAUTRIDOU, J. C. and PINEAU, A. (1981) *Engng. Fract. Mech.*, **15**, 55–71.
(12) MARINI, B., MUDRY, F., and PINEAU, A. (1985) *Engng. Fract. Mech.*, **22**, 989–996.
(13) ARGON, A. S., IM, J., and SAFOGLU, R. (1975) *Met. Trans.*, **6A**, 825–837.
(14) RICE, J. R. and TRACEY, D. M. (1969) *J. Mech. Phys. Solids*, **17**, 201.
(15) PERRIN, G. and LEBLOND, J. B. Analytical study of a hollow sphere made of porous plastic material and subjected to hydrostatic tension – application to some problems in ductile fracture of metals, Submitted to *Int. J. Plasticity*.
(16) GURSON, A. L. (1977) *J. Engng. Mat. Mech.*, **99**, 2–15.
(17) TVERGAARD, V. (1981) *Int. J. Fracture*, **17**, 389.
(18) NEEDLEMAN, A. (1989) Computational micromechanics, *Theoretical and applied mechanics* (Edited by P. Germain *et al.*), Elsevier Science Publishers, 217–240.
(19) TVERGAARD, V. and NEEDLEMAN, A. (1984) *Acta Metall.*, **32**, 157.
(20) MUDRY, F. (1982) *Etude de la rupture ductile et de la rupture par clivage d'aciers faiblement alliés*, Thesis.
(21) HANCOCK, J. W. and BROWN, D. K. (1983) *J. Mech. Phys. Solids*, **31**, 1–24.
(22) THOMSON, R. D. and HANCOCK, J. W. (1984) Deformation of porous imperfections relevant to ductile fracture, *Proceedings ICF6*, New Dehli, Vatluri Ed, **2**, 1321–1327.
(23) ROUSSELLIER, G. (1979) *Contribution à l'étude de la rupture des métaux dans le domaine de l'élasto-plasticité*, Thesis, Ecole Polytechnique.
(24) ROUSSELIER, G. (1987) *Nucl. Engng Des.*, **105**, 97–11.
(25) RICE, J. R. and JOHNSON, M. A. (1970) The role of large crack tip geometry changes in plane strain fracture, *Inelastic Behaviour of Solids* (Edited by M. F. Kannimen *et al.*), McGraw-Hill, New York, 641.
(26) McMEEKING, R. M. (1977) *J. Mech. Phys. Solids*, **25**, 357.
(27) HUTCHINSON, J. W. (1968) *J. Mech. Phys. Solids*, **16**, 13–31.
(28) RICE, J. R. and ROSENGREN, G. F. (1968) *J. Mech. Phys. Solids*, **16**, 1–12.
(29) WALLIN, K. (1984) *Engng. Fract. Mech.* **19**, 1085–1093.
(30) WALLIN, K. (1985) *Engng. Fract. Mech.* **22**, 149–163.
(31) GARWOOD, S. J. (1982) *Int. J. Presure Vessels Piping*, **10**, 297–319.
(32) ROOS, E., EISELE, U., SILCHER, H., and KIESSLING, D. (1987) Determination of J curves by large scale specimen, *13MPA Seminar*, MPA, Stuttgart (W. G.).
(33) MARANDET, B., PHELIPPEAU, G., DE ROO, G., and ROUSSELIER, G. (1984) Effect of specimen dimensions on J_{IC} at initiation of crack growth by ductile tearing, *Fracture Mech.: Fifteenth Symposium, ASTM STP 833*, ASTM, Philadelphia.

(34) MUDRY, F., DI RIENZO, F., and PINEAU, A. (1989) Numerical comparison of global and local criteria in compact tension and centre-crack panel specimens, *ASTM STP 995*, pp. 24–39 ASTM, Philadelphia.
(35) ROUSSELIER, G., DEVESA, G., and BETHMONT, M. (1989) Effect of specimen geometry on *J* resistance curves in near small-scale yielding condition, *Proceedings ICF7 Conf. Houston* (Edited by K. Salama), Pergamon Press, **1**, 249–258.
(36) TRAUTWEIN, A. and GYSEL, W. (1986) Influence of a long time aging of CF8 and CF8M cast steel at temperatures between 300 and 500°C on the impact toughness and the structure properties, *ASTM STP 756*, p. 165, ASTM, Philadelphia.
(37) SLAMA, G., PETREQUIN, P., and MAGER, T. (1983) Effect of aging on mechanical properties of austenitic stainless steel castings and welds, *SMIRT Post Conf. Seminar*, Monterey.
(38) CHOPRA, O. K. and CHUNG, H. M. (1985) *Nucl. Engng. Des.*, **89**, 305–318.
(39) VRINAT, M., COZAR, R., and MEYZAUD, Y. (1986) *Scripta Metall.*, **20**, 1101–1106.
(40) JOLY, P. (1988) *Approche locale de la rupture d'un matériau biphasé: austenite ductile et ferrite fragile, Diplome d'Etudes Approfondies*, Centre des Matériaux Ecole des Mines.
(41) COZAR, R. Private communication.
(42) WRAY, P. J., RICHMOND, O., and MORRISON, H. L. (1983) *Metallography*, **16**, 39–58.
(43) SPITZIG, W. A., KELLY, J. F., and RICHMOND, O. (1985) *Metallography*, **18**, 235–261.
(44) SCHWALBE, K. H., NEALE, B. K., and INGHAM, T. (1988) *Fatigue Fracture Engng. Mater Structures.*, **11**, 409–420.